Earth and Planetary Science Letters 439 (2016) 81–87

Contents lists available at ScienceDirect

Earth and Planetary Science Letters

www.elsevier.com/locate/epsl

Segment-scale volcanic episodicity: Evidence from the North Kolbeinsey Ridge, Atlantic

I.A. Yeo [a,*], C.W, Devey [a], T.P. LeBas [b], N. Augustin [a], A. Steinführer [a]

[a] GEOMAR Helmholtz Institute for Ocean Research Kiel, D-24148 Kiel, Germany
[b] National Oceanography Centre, Southampton, UK

ARTICLE INFO

Article history:
Received 24 August 2015
Received in revised form 20 January 2016
Accepted 24 January 2016
Available online 4 February 2016
Editor: C. Sotin

Keywords:
Mid-Atlantic Ridge
slow-spreading ridge
autonomous underwater vehicle
sidescan sonar
sea-floor spreading
volcanism

ABSTRACT

The upper oceanic crust is produced by magmatism at mid-ocean ridges, a process thought to be characterized by cyclic bouts of intense magmatic activity, separated by periods when faulting accommodates most or even all of the plate motion. It is not known whether there is a distinct periodicity to such magmatic–tectonic cycles. Here we present high-resolution sidescan sonar data from the neovolcanic zone of the North Kolbeinsey Ridge, a shallow slow-spreading ridge where high glacial and steady post-glacial sedimentation rates allow relative flow ages to be determined with a resolution of around 2 kyr using backscatter amplitude as a proxy for sediment thickness and hence age. We identify 18 lava flow fields covering 40% of the area surveyed. A group of 7 flow fields showing the highest (and similar) backscatter intensity are scattered along 75 km of axial valley surveyed, suggesting that at least this length of the segment was magmatically active within a 1.2 kyr time window. Based on conservative age estimates for all datable flows and estimated eruption volumes, the post-glacial volcanic activity imaged is insufficient to maintain crustal thickness, implying that episode(s) of enhanced activity must have preceded the volcanism we image.

1. Introduction

1.1. Volcanic periodicity on slow-spreading mid-ocean ridges

At slow-spreading ridges, episodes of volcanism are likely to be separated by periods of relative magmatic quiescence, when fault movement accommodates plate separation. This interplay between volcanism and tectonism controls Layer 2A growth (Escartín et al., 2007) and possibly the fractionation state and heterogeneity shown by mid-ocean ridge lavas (Rubin and Sinton, 2007). The periodicity of magmatic periods may be controlled directly by melt supply to the ridge (Parson et al., 1993), or be influenced by external factors like sea level and orbital eccentricity (Tolstoy, accepted; Crowley et al., 2015), although climatic forcing is unlikely to increase volcanic activity by more than around 50%. Estimates of cycle lengths vary from tens of thousands of years (Bryan and Moore, 1977; Sinha et al., 1998; Ballard and Van Andel, 1977) to hundreds of thousands of years (Searle et al., 1998; Mendel et al., 2003) with variable estimates for periods at intermediate-spreading ridges (6 kyr, Clague et al., 2014), fast spreading ridges (tens of kyr to ten of years, Bowles et al., 2006 and Sinton et al., 2002) and the Galapagos Spreading Centre, which is underlain by a hotspot (hundreds of years, Bowles et al., 2014). Scatter is due to difficulty in accurately dating young volcanic events and detecting individual flows, and because process rates are a function of the measured time interval (Gardner et al., 1987). There are very few mid-ocean ridges for which we have any knowledge of the eruption history over a relevant period of time. Individual lava flow fields have been successfully mapped and measured using repeat bathymetric surveying (Caress et al., 2012; Fox et al., 1992) but radiometric dating of these flows (e.g. Duncan and Hogan, 1994) and reconstruction of geological histories is commonly limited by the sample density. Others have used sediment drape thickness as a proxy for age (Mitchell, 1993, 1995a) using data from both sub-bottom profilers and sidescan sonar to differentiate relatively large differences in drape thickness. Paleomagnetic studies have also provided useful age information (e.g. Schouten et al., 1999), but require near bottom magnetometer surveys, while some successful work has been done using geomagnetic paleointensity of submarine basaltic glasses (Bowles et al., 2005).

Deep submergence, high-frequency sidescan sonar has, in regions with well constrained sedimentation rates, the potential to simultaneously yield information on both flow field ages and their areal extents and distribution. Beam penetration into sediment at frequencies of 120 kHz is physically limited to <2 m

* Corresponding author.
E-mail address: iyeo@geomar.de (I.A. Yeo).

http://dx.doi.org/10.1016/j.epsl.2016.01.029

(Mitchell, 1993) and in practice is probably only a few tens of centimeters, so centimeter scale differences in sediment thickness should be detectable in the sonar reflectivity of lava flows.

1.2. Geological setting

The Kolbeinsey Ridge (KR) is a region of the Mid-Atlantic Ridge between 66.5°N and 71.7°N, bounded to the north and south by the Jan Mayen and Tjörnes Fracture Zones, respectively. It has been an active slow-spreading centre since at least 26 Ma (Brandsdóttir et al., accepted; Bott, 1985) with a rate of <20 mm/yr since 9.5 Ma (Vogt et al., 1980; Kodaira et al., 1998). The ridge is divided by non-transform offsets into three segments ("North", "Central" and "South"), all of which are unusually shallow and have abnormally thick crust, perhaps as a result of higher mantle temperatures close to the Iceland hotspot (Vogt et al., 1980; Kodaira et al., 1998) and/or the effects of mantle compositions (Haase et al., 2003). The relatively steady post-glacial sedimentation rates (~2 cm/kyr Nowaczyk and Frederichs, 1999) and thickened crust (implying excess magmatism) make the Northern Kolbeinsey Ridge (NKR) an ideal place for application of the sidescan dating method.

1.3. Sedimentary history of the Kolbeinsey Ridge

Knowledge of the sediment type and sedimentation rates is necessary to estimate sediment thicknesses and derive lava flow ages. No sediment core data directly from the Northern Kolbeinsey Ridge are available but numerous cores have been taken in the surrounding region. Cores taken from further south on the ridge (between 67.04°N and 67.22°N, 100 km from the Icelandic coast) contain a combination of volcaniclastic material and sands, silts, muds and clays, predominantly derived from Iceland (Lackschewitz and Wallrabe-Adams, 1991). As the NKR lies 180 km from Jan Mayan and almost 600 km from Iceland sedimentation on the NKR is probably dominated by the finer grained muds and silts found in cores further north (Thiede and Hempel, 1991). The last glaciation, ending approximately 10–15 ka (Ruddiman and McIntyre, 1981) has resulted in variable sedimentation rates over the last few tens of thousands of years. Paleointensity measurements on cores within 200 km of the study area (69.5°N to 70.25°N) by Nowaczyk and Frederichs (1999) show sedimentation rates of 2 cm/kyr from 1 to 11 ka, 5 cm/kyr from 11 to 13 ka, 3.7 cm/kyr from 13 to 30 ka and 2 cm/kyr prior to 30 ka.

2. Materials and methods

Data were collected on cruise POS436 of the German research vessel F.S. Poseidon in June/July 2012. Ship multibeam bathymetry was acquired using the onboard Seabeam SB3050 echosounder. Initial collection and processing were done using the Hypack and Hysweep software packages. Final cleaning and griding (at 35 m cell size) of the maps was conducted in Fledermaus. A latency issue in the system (caused by a non-constant time offset between the echo-sounder and GPS) that was only discovered late in the cruise and could not be eliminated while at sea led to some offset in the absolute positioning of individual multibeam pings. We used the NavAdjust feature of MB-System (Caress, 1999) to re-align all survey lines and to produce a final, integrated grid.

AUV side-scan data were acquired using GEOMAR's REMUS6000 vehicle "ABYSS" and its Edgetech 2200-MP s120 kHz CHIRP (Compressed High-Intensity Radar Pulse) sidescan sonar running at 120 kHz. The CHIRP pulse has a bandwidth of 12 kHz and a beam width of 0.2° resulting in horizontal resolutions across-track (perpendicular to vehicle heading) of 0.625 m and along track of between 0.17 and 1.7 m. The sidescan mosaics were produced with 2 m pixels and with 100% coverage. The sidescan sonar measures only sonar reflectivity and no sub-bottom information is collected. Mosaics of the data were produced using Chesapeake SonarWiz software. Additional mosaics and all beam amplitude measurements used for the acoustic age assessments were extracted using PRISM (Le Bas and Huvenne, 2009) in areas of flat seafloor within the boundaries of individual mapped flows.

3. Results and discussion

3.1. Axial morphology

Our bathymetric map (Fig. 1A) allows the location of the NKR spreading axis to be determined in detail for the first time. It has a relatively simple axial structure north of 71°15′N, characterized by a normal-fault-bounded axial valley containing numerous flat-topped seamounts (Fig. 1B). The central section as far south as 70°55′N, with the exception of Eggvin Bank volcano, is mostly smooth, with ca. 70% of the seafloor having a rugosity value (the ratio of the actual 3D area divided by the area if flat) of <1.05. This distribution of volcanic terrains is atypical of slow-spreading ridges, which generally comprise a high percentage of rugose hummocky volcanics (Smith and Cann, 1990). The southern end of the NKR shows two parallel volcanic zones separated by a 10 km wide ridge of tectonized seafloor. An oblique valley, bounded by normal faults and containing lava flows, appears to connect the westernmost of the valleys with the main ridge to the north. It is not possible to say definitively whether this area is an overlap with the Central Kolbeinsey Ridge, an evolving partial-segment jump or a double axial valley. However, there is no evidence for the faults curving towards each other, as might be expected in an overlapping spreading centre (e.g. Klein et al., 2013) and there appear to be more volcanic features in the eastern valley, which aligns with the main ridge trend to the north, suggesting an evolving ridge jump of this small section westwards towards the Central Kolbeinsey Ridge is probably the most likely explanation. Eggvin Bank Volcano is located on the intersection of the oblique valley with the main ridge trend to the north. It also lies on top of the major eastern axial valley wall bounding fault along this section of the ridge.

The 145 flat-topped seamounts imaged have an average diameter of 1100 m and an average height above the surrounding seafloor of 114 m, and so conform to the typical 1:10 height:diameter ratio observed elsewhere (Smith et al., 1995a, 1995b) and for seamounts over 50 m in height display a similar exponential size-frequency distribution to that observed both on the Reykjanes Ridge (Magde and Smith, 1995) and the regions of the Galapagos spreading centre which possess a rift valley (Behn et al., 2004). The hummocky volcanics (Fig. 1B) have an average flow-unit thickness of 30 m based on their relief in the bathymetric maps (ranging from ≤10 to 85 m), thinner than hummocky seamounts on the Reykjanes Ridge (Magde and Smith, 1995).

3.2. Sidescan lava flow mapping and relative ages

Six areas (covering 20% of the neovolcanic zone) were chosen for sidescan surveying by AUV (Fig. 1A). In these areas, 60% of the seafloor shows low acoustic backscatter, with no evidence of recent volcanic activity. The remaining 40% consists of lava flow fields with higher backscatter, indicating the presence of hard substrate that, in a mid-ocean ridge environment, is lava. We distinguish 18 lava-covered regions with areas between 0.3 km^2 and 15.8 km^2 (Fig. 2). As it is not possible to determine whether these individual regions represent single lava flows or are each comprised of several flow units, we use the term "flow field" here to describe them. Information about the lava surface morphologies is also visible in

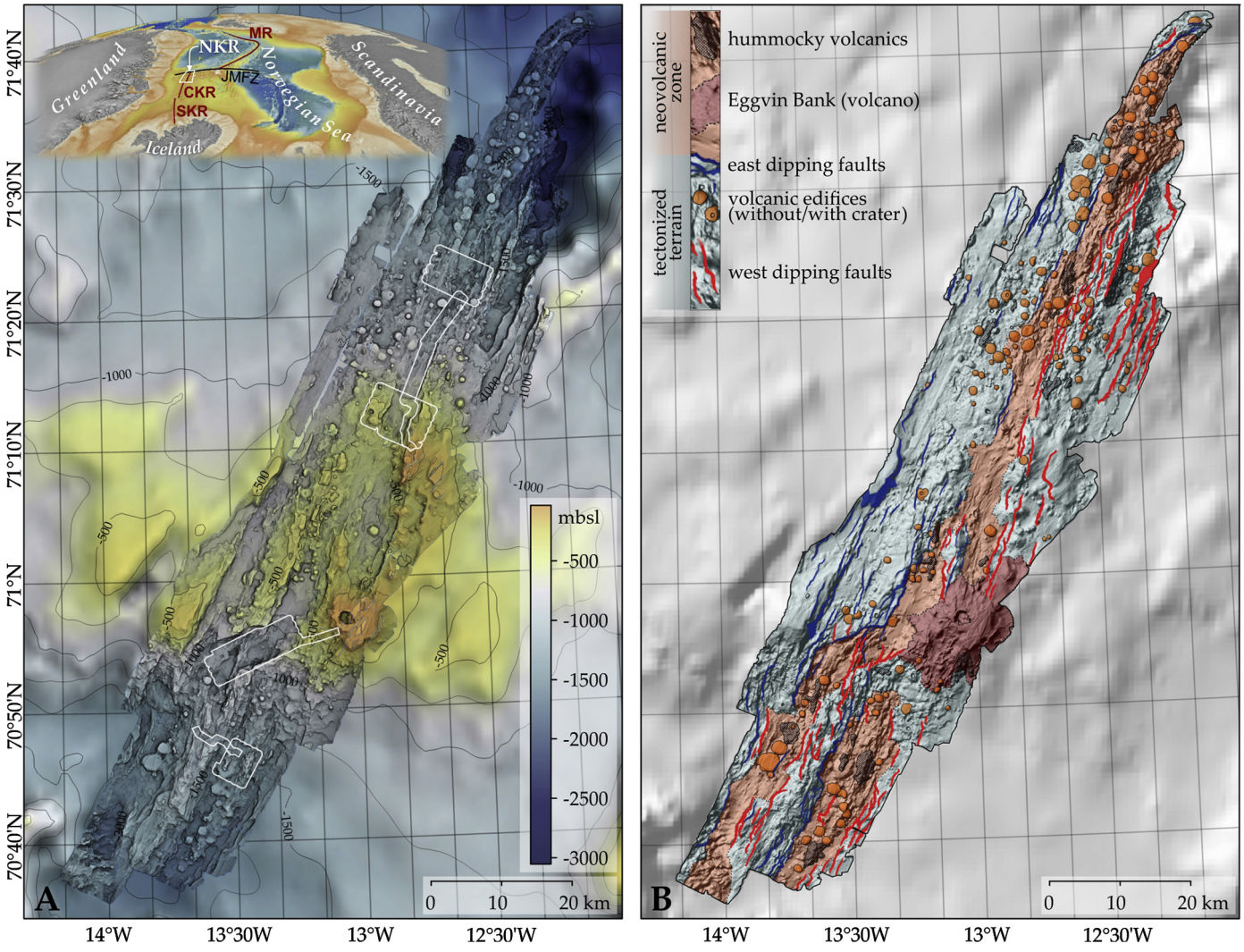

Fig. 1. (A) SB3050 multibeam Tedain Texture Shaderr bathymetry of the Northern segment of the Kolbeinsey Ridge gridded at 50 m (B) geological map based on the bathymetry and sidescan sonar data. Terrain Texture Shader (TTS) maps use an algorithm to produce maps with a hierarchical framework that emphasizes details with no dependence on lighting direction. The white boxes mark the areas covered by AUV sidescan sonar surveys and correspond to the surveys shown in Fig. 2 (which shows all 6) and Fig. 3 (which shows only the survey in the oblique valley). Inset: Tectonic setting of the North Kolbeinsey Ridge (NKR) The Central Kolbeinsey Ridge (CKR) South Kolbeinsey Ridge (SKR), Mohns Ridge (MR) and the Jan Mayan Fracture Zone (JMFZ) are labeled. Eggvin Bank Volcano lies on the boundary between the Central Kolbeinsey and Northern Kolbeinsey Ridges.

the sidescan imagery (e.g. Fig. 3). Unlike 25°N on the Mid-Atlantic Ridge, where smooth seafloor is pillowed (Cann and Smith, 2005) we conclude the majority of the flow fields mapped by sidescan sonar are likely to be massive sheet or lobate flows, as these regions also display both tumuli and collapsed lava surface crusts, characteristic features of sheet or lobate flows.

The flow fields show different backscatter intensities. While this could be due to variations in the thickness of their sediment cover (and hence age), we must first remove variations resulting from differences in any or all of the following factors: (A) absorption of the signal in water, (B) the overlying sediment type, (C) the angles ("grazing angles") at which the beams meet the seafloor, and (D) surface roughnesses of the different flow fields. Operationally, we minimized (A) by ensuring that all surveys were performed at a constant (low) vehicle altitude (50 ± 10 m) keeping acoustic range small. In this deep-sea setting, variation in sediment type should be limited and this is supported by the lack of variation in the amplitudes measured in background areas, so grain-size effects (B) can be discounted. By using only data from flat seafloor (i.e. seafloor with a slope $<5°$ based on our multibeam maps) the grazing angle becomes a simple function of distance from the sound source, making it easy to compare data with the same grazing angles (C). The effects of surface roughness variations (D) are more difficult to deal with, especially the smaller scale roughness, which may lead to lava outcropping through thin sediment blankets. The effect of larger scale surface roughness variations can be obviated by using the sidescan imagery to compare similar flow types (i.e. choose only the smooth centre of sheet flows), but, in the absence of visual observations of the seafloor, we need to assume that, at the length scale sampled by our backscatter analysis (see below) all sheet flows have a similar form of surface microstructure.

Because sediment thickness on flow surfaces naturally varies to some extent we average data from 50 consecutive pings along-track (equivalent to 15–20 m on the seafloor), fitting a 5-point moving curve to this average (smoothing the data over an across-track distance of approximately 3.1 m) and then pooling average data from at least 4 different areas on any one flow. We assume that sedimentation rate is uniform across the area studied.

Fig. 4 shows the resulting backscatter amplitude profiles. Measured amplitudes are consistently higher and less noisy on the port side due to inherent sensitivity differences in the hardware, so we compare only port-side profiles in the following discussion. "Back-

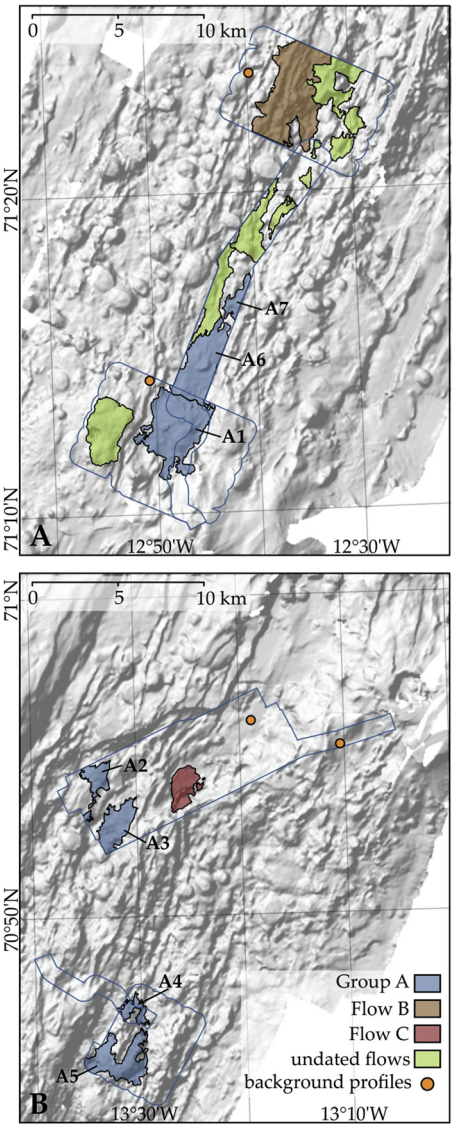

Fig. 2. Enlarged multibeam bathymetry illuminated from the northwest showing AUV sidescan sonar coverage (blue outlines) with the lava flow fields mapped from these datasets shown in color. Group A lavas are shown in blue, Flow B in brown and Flow C in red. Note the large along axis distribution of Group A flow fields. (For interpretation of the references to color in this figure legend, the reader is referred to the web version of this article.)

ground" backscatter amplitude was determined at several flat, featureless off-axis areas (locations shown in Fig. 2) where sediment cover is too thick for the sonar to see through and should therefore result only from sound being reflected at the sediment/water interface with variation due to the other factors listed and/or fading (Mitchell, 1995b). The highest measured value is used as the reference value for all sediment thickness calculations.

We were able to extract backscatter profiles fitting our selection criteria from 9 of the 18 flow fields mapped (Figs. 2 and 4D). Those flow fields for which profiles could not be extracted were either (a) narrower than the AUV sidescan swath, resulting in incomplete profiles, (b) too small for multiple profiles to be measured, or (c) had no smooth areas large enough to extract full profiles. Amplitude curves were compared between 50 and 200 m away from the vehicle, where the grazing angles are steepest and so differences in sediment cover should be most clearly visible. Using the ratios of the amplitudes of the flow fields to our lowest background value (equivalent to total attenuation of the beam excluding the first reflection), alongside attenuation values for muddy sediments from Hamilton (1980), we are able to calculate the sediment thickness differences between the flow fields and the highest measured value for Group A (Appendix 1) as: 6.4 cm for Flow Field C, 3.6 cm for Flow Field B, 2.3 cm for the minimum Group A, and 16.0 cm for the background. Using a sedimentation rate of 2 cm/kyr (assuming rates from Nowaczyk and Frederichs, 1999 are accurate) the total range imaged is 16 cm, equivalent to 8 kyr. The difference in age between Flow Field C and Flow Field B is around 1.4 ka, and between Flow Field B and the lowest values for Group A is 0.7 ka. The entire Group A was erupted in a period <1.2 kyr. Assuming Group A are zero age, supported by the fact these flows are unfaulted and flow around and over older tectonic features (e.g. flow field A2, which flows around faults at its northern end and crosses several small fissures (Fig. 3)) we imaged no flows older than 3.2 kyr and the maximum age resolved with this method is 8 kyr. This would be larger if the Group A lavas are not recent. These calculations are heavily dependent on a number of assumptions including assuming that the sediment drape and the surface structure of the lava flow fields are homogeneous, that sedimentation rate is constant through time and that the effects of acoustic refraction within the sediment are negligible. Sediment thickness may be overestimated if the sediments are sandier than assumed, though not greatly, for example using values for a sandy silt (Hamilton, 1980) the total thickness from lowest background to maximum Group A is 11 cm (Appendix 1).

Estimating a vertical resolution for this method is difficult without a calibrated reference value. The vertical resolution of a sub bottom profiler with a 12 kHz bandwidth would be around 7 cm, however our resolution is better than this as we are clearly able to distinguish Flow Fields A2 and A3 from Flow Field C, and they are different well outside of the typical scatter of a single curve, despite our calculated sediment thickness between them being only 4.2 cm. The scatter in the background values should represent errors resulting from all variables except sediment thickness and lava flow surface roughness (because there is no lava flow being imaged). In this case these variations are equivalent to around 4 cm of sediment thickness (Appendix 1), although even this seems to be an overestimation of what we are able to distinguish. Regardless, a 4 cm resolution (equivalent to ± 1 kyr at a sedimentation rate of 2 cm/kyr) would allow us to class Flow C and Group A as different from each other and the background, but is greater than the sediment cover differences between Flow B and either Group A or Flow C.

3.3. Magmatic episodicity at North Kolbeinsey

Group A lavas are found along 75 km of axis surveyed, suggesting that this length of the axis was active in the same 1.2 kyr period. The shallow NKR segment centre and its almost completely unfaulted neovolcanic zone (see Fig. 1) are similar to features seen at fast-spreading ridges hosting a melt body (e.g. Phipps Morgan and Chen, 1993) and such a melt body may have fed flow fields in a manner similar to that predicted by some cyclic models (Parson et al., 1993). In these models, the supply of a batch of melt to the ridge axis results in large, long run-out eruptions, which focus and decrease in volume as the melt body solidifies

AUV survey areas were chosen to be representative of bathymetric features along the entire axis. Although this has limitations, it should yield the most representative information in the absence of total axial coverage. If we extrapolate the 20% volcanic coverage observed in our AUV surveys to the entire ridge axis, the total volume of all volcanic products in the NKR neovolcanic zone (sheet flow fields, hummocks and flat-topped volcanoes, see Fig. 1) is insufficient to account for crustal production in post-glacial times. To produce seismic layer 2A (the section of the crust thought to be composed of extrusive volcanics) with 0.65 km thickness (vary-

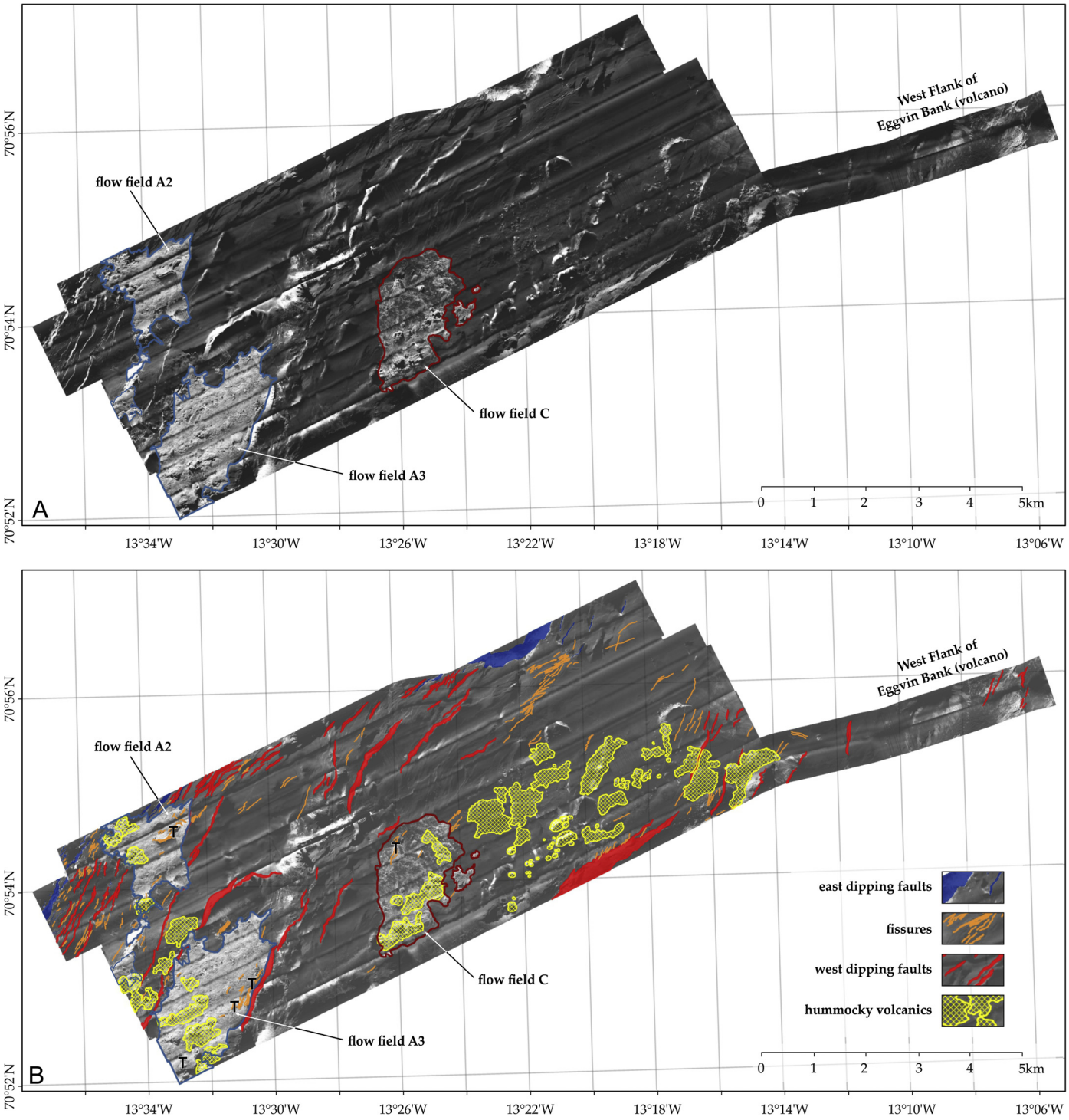

Fig. 3. (A) Mosaic of one of the AUV sidescan sonar datasets in which lava flow fields with differing backscatter strengths (corresponding to Fig. 4C) can clearly be seen. Imagery was processed and mosaicked using PRISM (Le Bas and Huvenne, 2009) and the SonarWiz processing package. Ensonification from the northwest. (B) geological interpretation of the sidescan bathymetry. The cluster of hummocky volcanics around 1318'W 70°55′W may be an older lava field, now too covered by sediment to accurately pick the boundaries. Locations of major tumuli are shown with a letter "T".

ing from 0.5–0.8 along axis Kodaira et al., 1997) at a full spreading rate of 1.8 cm/yr within the last 8 kyr requires approximately 13.1 km^3 of lava to be erupted along the 140 km-long segment. This is slightly higher than the range of rates required to maintain typical 2A thicknesses of 0.1–0.5 km (Peirce et al., 2007) on the southern Reykjanes Ridge (for the same segment length and a full spreading rate of 21.5 mm/yr this layer 2A thickness would require between 2.4 and 12.0 km^3 of lava to be erupted over the same period). The total area of the flow fields we mapped (Fig. 2) is 78.4 km^2. As these flow fields show no positive bathymetric signature, their thickness is likely to be similar to or less than the vertical resolution of our multibeam mapping system, conservatively estimated at 10 m. This is in accordance with observations on slow-spreading ridges elsewhere e.g. Karson et al. (2002) although thicker flows are observed on Iceland and the fast spreading East Pacific Rise. Using this thickness estimate, the flow fields have a

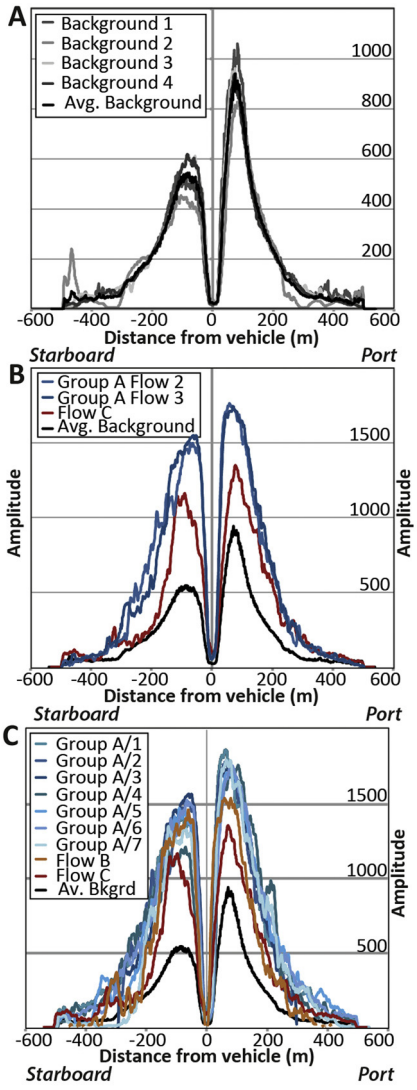

Fig. 4. Amplitude profiles (no units given as amplitude is not calibrated on the AUV) for (A) four background areas and their average, (B) the lava flow fields shown in Fig. 3, and (C) all the lava flow fields on the segment for which smooth profiles could be extracted.

volume of 0.78 km^3. Extrapolated to the entire axis, sheet flow fields contribute 3.9 km^3. Hummocks are observed on less than 10% (57 km^2) of the neovolcanic zone with a volume of 2.7 km^3. We have no age constraints from sediment thickness for the hummocks and so use the valley width of 3.5 km combined with the spreading rate to define their age as $\leq$200 ka, equating to an eruption rate of 0.14 km^3/10 ka (0.01 km^3 in the last 8 kyr). Similar assumptions are applied to the 145 flat-top seamounts mapped, of which 40 (total volume of 6.1 km^3) lie within the inner valley, yielding a production rate of. 0.31 km^3/10 ka (0.25 km^3/8 kyr). Additional volcanic input from Eggvin Bank Volcano is excluded as there is no evidence that large volume flows are reaching the main axial valley (Fig. 1, Fig. 3). The exception to this are possible Eggvin Bank flows filling the graben directly to the north of the volcano. Additionally, the volcano extents are picked from the break in slope, but may extend deeper than shown. However, any additional Eggvin flow volume would be small compared to the volumes required to noticeably change the estimated volcanic imput from the segment and the trace of the volcano off axis suggests the crust here is locally thickened compared to the rest of the segment meaning that this region may also have a thicker extrusive volcanic section not accounted for in the average seismic 2A crustal thickness.

Summing these estimates, only 4.16 km^3 or around 32% of the volume required to maintain crustal thickness for the last 8 kyr is accounted for. This is equivalent to 0.5 km^3 per kyr, around 10% of that observed during the last 10 ka in the Western Volcanic Zone of Iceland (Sinton et al., 2005). The 8 kyr number is taken from the calculations in section 3.2 as the maximum penetration of our method and is therefore subject to the same assumptions, however, in order for there to not be a deficit in erupted material it would need to be less than 2.5 kyr, well outside errors likely due to sediment type or sediment rate variations. If 8 kyr underestimates the time span over which we can detect lava, eruption rates may be even lower. Additionally, if our estimate of sheet flow thickness were an underestimate, to account for the 13.1 km^3 of magma required to generate the crust over this time period a flow thickness of around 40 m would be required. Such flows would be much thicker than those on Iceland (e.g. McDougall et al., 1977) and the fast-spreading East-Pacific Rise (e.g. Macdonald et al., 1989) and should be visible on bathymetric maps.

4. Conclusions

The NKR axis appears to have experienced below-average post-glacial extrusive volcanic activity, in agreement with recent suggestions that high Holocene sea level and low-orbital eccentricity suppress mid-ocean ridge volcanism (Tolstoy, accepted; Crowley et al., 2015). To maintain the thickness of layer 2A long term, more intense magmatic episodes, and hence a episodicity of magmatism, are required. Whether this episodicity is magmatically or climatically driven will only become clear from examining segment-scale eruptive records spanning longer time periods, although climatic forcing is unlikely to account soley for the disparity.

At the NKR episodic magmatic episodes, comprising numerous volcanic eruptions along the ridge segment appear to occur on at least a tens of thousands of years timescale, similar to estimates for magma chamber volume at the RAMASSES area on the Reykjanes Ridge (Sinha et al., 1998) which suggested 30 kyr episodicity. Such high-volume, episodic magmatic events, rather than constant low level extrusive volcanism, are likely to occur globally on slow-spreading mid-ocean ridges.

Acknowledgements

The authors thank the scientific party, officers and crew of cruise POS436 for their professionalism and dedication. The AUV Abyss engineers, particularly Marcel Rothenbeck, provided expert support during deployments and method development. We thank Dean Wilson for his expertise in geophysical methods. We are grateful for careful and detailed comments from Neil Mitchell, Deborah Smith and three anonymous reviewers, which greatly improved the manuscript. IAY gratefully acknowledges the receipt of a Humboldt Foundation postdoctoral fellowship.

Appendix A. Supplementary material

Supplementary material related to this article can be found online at http://dx.doi.org/10.1016/j.epsl.2016.01.029.

References

Ballard, R.D., Van Andel, T.H., 1977. Morphology and tectonics of the inner rift valley at lat 36°50'N on the Mid-Atlantic Ridge. Geol. Soc. Am. Bull. 4, 507–530. http://dx.doi.org/10.1130/0016-7606.

Behn, M.D., Sinton, J.M., Detrick, R.S., 2004. Effect of the Galápagos hotspot on seafloor volcanism along the Galápagos Spreading Center (90.9–97.6°W). Earth Planet. Sci. Lett. 217 (3–4), 331–347. http://dx.doi.org/10.1016/S0012-821X(03)00611-3.

Bott, M.H.P., 1985. Plate tectonic evolution of the Icelandic Transverse Ridge and adjacent regions. J. Geophys. Res. 90 (B12), 9953. http://dx.doi.org/10.1029/JB090iB12p09953.

Bowles, J.A., Colman, A., Mcclinton, J.T., Sinton, J.M., White, S.M., Rubin, K.H., 2014. Eruptive timing and 200 year episodicity at 92°W on the hot spot-influenced Galapagos Spreading Center derived from geomagnetic paleointensity. Geochem. Geophys. Geosyst. 15, 2211–2224. http://dx.doi.org/10.1002/2014GC005315. Received.

Bowles, J., Gee, J.S., Kent, D.V., Bergmanis, E., Sinton, J., 2005. Cooling rate effects on paleointensity estimates in submarine basaltic glass and implications for dating young flows. Geochem. Geophys. Geosyst. 6 (7). http://dx.doi.org/10.1029/2004GC000900.

Bowles, J., Gee, J.S., Kent, D.V., Perfit, M.R., Soule, S.A., Fornari, D.J., 2006. Paleointensity applications to timing and extent of eruptive activity, 9°–10°N East Pacific Rise. Geochem. Geophys. Geosyst. 7 (6). http://dx.doi.org/10.1029/2005GC001141.

Brandsdóttir, B., Hooft, E.E.E., Mjelde, R., Murai, Y., accepted. Origin and evolution of the Kolbeinsey Ridge and Iceland Plateau, N-Atlantic. Geochem. Geophys. Geosyst. http://dx.doi.org/10.1002/2014GC005540.

Bryan, W.B., Moore, J.G., 1977. Compositional variations of young basalts in the Mid-Atlantic Ridge rift valley Compositional variations of young basalts in the Mid-Atlantic Ridge rift valley near lat 36°49'N. Geol. Soc. Am. Bull. 4, 556–570. http://dx.doi.org/10.1130/0016-7606(1977)88<556.

Cann, J.R., Smith, D.K., 2005. Evolution of volcanism and faulting in a segment of the Mid-Atlantic Ridge at 25°N. Geochem. Geophys. Geosyst. 6 (9). http://dx.doi.org/10.1029/2005GC000954.

Caress, D.W., 1999. MB-System – public domain software for processing swath mapping sonar data. Undersea Explorations.

Caress, D.W., Clague, D.A., Paduan, J.B., Martin, J.F., Dreyer, B.M., Chadwick, W.W., Denny, A., Kelley, D.S., 2012. Repeat bathymetric surveys at 1-metre resolution of lava flows erupted at Axial Seamount in April 2011. Nat. Geosci. 5 (7), 483–488. http://dx.doi.org/10.1038/ngeo1496.

Clague, D.A., Dreyer, B.M., Paduan, J.B., Martin, J.F., Caress, D.W., Guilderson, T.P., Mcgann, M.L., 2014. Geochemistry, Geophysics, Geosystems. Geochem. Geophys. Geosyst. 15 (8), 3364–3391. http://dx.doi.org/10.1002/2014GC005415.

Crowley, J.W., Katz, R.F., Huybers, P., 2015. Glacial cycles drive variations in the production of oceanic crust. Sciencexpress, 1–7. http://dx.doi.org/10.1126/science.1261508, February.

Duncan, R.A., Hogan, L.G., 1994. Radiometric dating of young MORB using the ^{40}Ar–^{39}Ar incremental heating method. Geophys. Res. Lett. 21 (18), 1927–1930. http://dx.doi.org/10.1029/94GL01375.

Escartín, J., Soule, S.A., Fornari, D.J., Tivey, M.A., Schouten, H., Perfit, M.R., 2007. Interplay between faults and lava flows in construction of the upper oceanic crust: The East Pacific Rise crest 9°25′–9°58′N. Geochem. Geophys. Geosyst. 8 (6). http://dx.doi.org/10.1029/2006GC001399.

Fox, C.G., Chadwick, W.W., Embley, R.W., 1992. Detection of changes in ridge-crest morphology using repeated multibeam sonar surveys. J. Geophys. Res. 97 (B7), 11149–11162. http://dx.doi.org/10.1029/92JB00601.

Gardner, T.W., Jorgensen, D.W., Shuman, C., Lemieux, C.R., 1987. Geomorphic and tectonic process rates: effects of measured time interval. Geology 15 (3), 259–261.

Haase, K.M., Devey, C.W., Wieneke, M., 2003. Magmatic processes and mantle heterogeneity beneath the slow-spreading northern Kolbeinsey Ridge segment, North Atlantic. Contrib. Mineral. Petrol. 144, 428–448. http://dx.doi.org/10.1007/s00410-002-0408-z.

Hamilton, E.L., 1980. Geoacoustic modeling of the sea floor. J. Acoust. Soc. Am. 65 (5), 1313–1340. http://dx.doi.org/10.1121/1.385100.

Karson, J.A., Tivey, M.A., Delaney, J.R., 2002. Internal structure of uppermost oceanic crust along the Western Blanco Transform Scarp: implications for subaxial accretion and deformation at the Juan de Fuca Ridge. J. Geophys. Res. 107 (B9), 1–23. http://dx.doi.org/10.1029/2000JB000051.

Klein, E.M., White, S.M., Nunnery, J.A., Mason-Stack, J.L., Wanless, V.D., Perfit, M.R., Waters, C.L., Sims, K.W.W., Fornari, D.J., Zaino, A.J., Ridley, W.I., 2013. Seafloor photo-geology and sonar terrain modeling at the 9°N overlapping spreading center, East Pacific Rise. Geochem. Geophys. Geosyst. 14 (12), 5146–5170. http://dx.doi.org/10.1002/2013GC004858.

Kodaira, S., Mjelde, R., Gunnarsson, K., 1997. Crustal structure of the Kolbeinsey North Atlantic, obtained by use of ocean bottom seismographs. J. Geophys. Res. 102 (B2), 3131–3151.

Kodaira, S., Mjelde, R., Gunnarsson, K., Shiobara, H., Shimamura, H., 1998. Evolution of oceanic crust on the Kolbeinsey Ridge, north of Iceland, over the past 22 Myr. Terra Nova 10, 27–31. http://dx.doi.org/10.1046/j.1365-3121.1998.00166.x.

Lackschewitz, K.S., Wallrabe-Adams, H.-J., 1991. Composition and origin of sediments on the mid-oceanic Kolbeinsey Ridge, north of Iceland. Mar. Geol. 101 (1–4), 71–82. http://dx.doi.org/10.1016/0025-3227(91)90063-A.

Le Bas, T.P., Huvenne, V.A.I., 2009. Acquisition and processing of backscatter data for habitat mapping – comparison of multibeam and sidescan systems. Appl. Acoust. 70 (10), 1248–1257. http://dx.doi.org/10.1016/j.apacoust.2008.07.010.

Macdonald, K.C., Haymon, R., Shor, A., 1989. A 220 km^2 recently erupted lava field on the East Pacific Rise near lat 8°S. Geology 17 (3), 212–216.

Magde, L.S., Smith, D.K., 1995. Seamount volcanism at the Reykjanes Ridge: relationship to the Iceland hot spot. J. Geophys. Res., Solid Earth 100 (B5), 8449–8468. http://dx.doi.org/10.1029/95JB00048.

McDougall, I., Saemundsson, K., Johannesson, H., Watckins, N.D., Kristjansson, L., 1977. Extension of the geomagnetic polarity time scale to 6.5 my: K–Ar dating, geological and paleomagnetic study of a 3500-m lava succession in western Iceland. Geol. Soc. Am. Bull. 88, 1–15.

Mendel, V., Sauter, D., Rommevaux-Jestin, C., Patriat, P., Lefebvre, F., Parson, L.M., 2003. Magmato-tectonic cyclicity at the ultra-slow spreading Southwest Indian Ridge: evidence from variations of axial volcanic ridge morphology and abyssal hills pattern. Geochem. Geophys. Geosyst. 4. http://dx.doi.org/10.1029/2002GC000417.

Mitchell, N.C., 1993. A model for attenuation of backscatter due to sediment accumulations and its application to determine sediment thicknesses with GLORIA sidescan sonar. J. Geophys. Res. 98 (B12), 22477–22493.

Mitchell, N.C., 1995a. Characterising the extent of volcanism at the Galapagos Spreading Centre using Deep Tow sediment profiler records. Earth Planet. Sci. Lett. 134 (3–4), 459–472. http://dx.doi.org/10.1016/0012-821X(95)00132-V.

Mitchell, N.C., 1995b. Representing backscatter fluctuations with a PDF convolution equation and its application to study backscatter variability in side-scan sonar images. IEEE Trans. Geosci. Remote Sens. 33 (6), 1328–1331. http://dx.doi.org/10.1109/36.477190.

Nowaczyk, N.R., Frederichs, T.W., 1999. Geomagnetic events and relative palaeointensity variations during the past 300 ka as recorded in Kolbeinsey Ridge sediments, Iceland Sea: indication for a strongly variable geomagnetic field. Int. J. Earth Sci. 88 (1), 116–131. http://dx.doi.org/10.1007/s005310050250.

Parson, L.M., Murton, B.J., Searle, R.C., Booth, D., Keeton, J., Laughton, A., Mcallister, E., Millard, N., Redbourne, L., Rouse, I., Shor, A., Smith, D., Spencer, S., Summerhayes, C., Walker, C., 1993. En echelon axial volcanic ridges at the Reykjanes Ridge: a life cycle of volcanism and tectonics. Earth Planet. Sci. Lett. 117, 73–87. http://dx.doi.org/10.1016/0012-821X(93)90118-S.

Peirce, C., Sinha, M., Topping, S., Gill, C., 2007. Morphology and genesis of slow-spreading ridges-seabed scattering and seismic imaging within the oceanic crust. Geophys. J. Int. 168 (1), 59–89. http://dx.doi.org/10.1111/j.1365-246X.2006.03223.x.

Phipps Morgan, J., Chen, Y.J., 1993. Dependence of ridge-axis morphology on magma supply and spreading rate. Nature 364, 706–708. http://dx.doi.org/10.1038/364706a0.

Rubin, K.H., Sinton, J.M., 2007. Inferences on mid-ocean ridge thermal and magmatic structure from MORB compositions. Earth Planet. Sci. Lett. 260 (1–2), 257–276. http://dx.doi.org/10.1016/j.epsl.2007.05.035.

Ruddiman, F.W., McIntyre, A., 1981. The North Atlantic Ocean during the last deglaciation. Palaeogeogr. Palaeoclimatol. Palaeoecol. 35 (0), 145–214. http://dx.doiorg/10.1016/0031-0182(81)90097-3.

Schouten, H., Tivey, M.A., Fornari, D.J., Cochran, J.R., 1999. Central anomaly magnetization high: constraints on the volcanic construction and architecture of seismic layer 2A at a fast-spreading mid-ocean ridge, the EPR at 9°30′–50′N. Earth Planet. Sci. Lett. 169 (1–2), 37–50. http://dx.doi.org/10.1016/S0012-821X(99)00063-1.

Searle, R.C., Cowie, P.A., Mitchell, N.C., Allerton, S., Macleod, C.J., Escartin, J., Russell, S.M., Slootweg, P.A., Tanaka, T., 1998. Fault structure and detailed evolution of a slow spreading ridge segment: the Mid-Atlantic Ridge at 298N. Earth Planet. Sci. Lett. 154, 167–183.

Sinha, M.C., Constable, S.C., Peirce, C., White, A., Heinson, G., MacGregor, L.M., Navin, D.A., 1998. Magmatic processes at slow spreading ridges: implications of the RAMESSES experiment at 57°45′N on the Mid-Atlantic Ridge. Geophys. J. Int. 135 (3), 731–745. http://dx.doi.org/10.1046/j.1365-246X.1998.00704.x.

Sinton, J., Grönvold, K., Saemundsson, K., 2005. Postglacial eruptive history of the Western Volcanic Zone, Iceland. Geochem. Geophys. Geosyst. 6 (12). http://dx.doi.org/10.1029/2005GC001021.

Sinton, J., Bergmanis, E., Rubin, K., Batiza, R., Gregg, T.K.P., Macdonald, K.C., White, S.M., 2002. Volcanic eruptions on mid-ocean ridges: new evidence from the superfast spreading East Pacific Rise, 17°–19°S. J. Geophys. Res. 107 (B6). http://dx.doi.org/10.1029/2000JB000090.

Smith, D.K., Cann, J.R., 1990. Hundreds of small volcanoes on the median valley floor of the Mid-Atlantic Ridge. Nature 348, 152–155. http://dx.doi.org/10.1038/348152a0.

Smith, D.K., Cann, J.R., Dougherty, M.E., Lin, J., Spencer, S., Macleod, C., Keeton, J., Mcallister, E., Brooks, B., Pascoe, R., Robertson, W., 1995a. Mid-Atlantic Ridge volcanism from deep-towed side-scan sonar images, 25°–29°N. J. Volcanol. Geotherm. Res. 67, 233–262.

Smith, D.K., Humphris, S.E., Bryan, W.B., 1995b. A comparison of volcanic edifices at the Reykjanes Ridge and the Mid-Atlantic Ridge at 24°–30°N. J. Geophys. Res. 100 (B11), 22485–22498.

Thiede, J., Hempel, G., 1991. Die Expedition ARKTIS-VII/1 mit FS "Polarstern". Rep. Polar Res. 80, 1–137.

Tolstoy, M., accepted. Mid-ocean ridge eruptions as a climate valve. Geophys. Res. Lett. http://dx.doi.org/10.1002/2014GL063015.

Vogt, P.R., Johnson, G.L., Kristjansson, L., 1980. Morphology and magnetic-anomalies north of Iceland. J. Geophys. 47 (1–3), 67–80.